


Contribution of exclusive $(\pi^0\pi^0, \pi^0\eta, \eta\eta)\gamma$ channels to the leading order HVP of the muon $g-2$

J. L. Gutiérrez Santiago^{✉*} and G. López Castro[†]

Departamento de Física, Centro de Investigación y de Estudios Avanzados del Instituto Politécnico Nacional, Apartado Postal 14-740, C.P. 07000 Ciudad de México, México

 (Received 23 May 2022; accepted 12 October 2022; published 28 October 2022)

We evaluate the contributions of $(\pi^0\pi^0, \pi^0\eta, \eta\eta)\gamma$ exclusive channels to the leading order hadronic vacuum polarization (HVP) of the muon anomalous magnetic moment. These final states can be viewed as decay subchannels in previous evaluations of the $\pi^0\omega$, $\eta\omega$, and $\eta\phi$ contributions to $a_\mu^{\text{had,LO}}$, where the vector resonances (decaying into $\pi^0/\eta + \gamma$) are assumed to be on-shell. Since the separation of resonance and background contributions in a given observable is, in general, a model-dependent procedure, here we use pseudoscalar mesons and the photon as the *in* and *out* states of the $e^+e^- \rightarrow (\pi^0\pi^0, \pi^0\eta, \eta\eta)\gamma$ S -matrix, such that the cross section contains the interferences among different contributions to the amplitudes. We find $a_\mu^{\text{had,LO}}(P_1^0 P_2^0 \gamma) = (1.17 \pm 0.13) \times 10^{-10}$, where uncertainties stem mainly from vector meson dominance model parameters. Improved experimental studies of these exclusive channels in the whole range below 2 GeV would reduce model-dependency.

DOI: [10.1103/PhysRevD.106.073009](https://doi.org/10.1103/PhysRevD.106.073009)

I. INTRODUCTION

During the last two decades, the most accurate measurements of the muon anomalous magnetic moment a_μ [1,2] have defied an explanation within the standard model (SM) framework. The reference value of a_μ in the SM prediction [3] lies 4.2σ below the average value of experimental results $\Delta a_\mu = a_\mu^{\text{exp}} - a_\mu^{\text{SM}} = 25.1(5.9) \times 10^{-10}$ [1–3], where theoretical and experimental uncertainties, 4.3 and 4.1×10^{-10} respectively, contribute with similar amounts [4–24]. The uncertainty in the theoretical value is dominated by input data used to evaluate the $O(\alpha^2)$ hadronic vacuum polarization (HVP) and also from evaluations of $O(\alpha^3)$ hadronic light-by-light (H-LbL) contributions. The experimental value includes the recent measurement of the Muon $g-2$ experiment [2], which is in good agreement with previous results from the BNL 821 collaboration [1]. Forthcoming experimental results from next runs at Fermilab as well as J-PARC [25] and PSI [26] will increase the accuracy reducing the current error by up to a factor of three [3].

The recent measurement of a_μ at Fermilab [2] arrived simultaneously with a new determination of the hadronic contributions based on lattice QCD [27]. This calculation claims to have reached an accuracy similar to the one of the reference value in the SM (dispersive calculation of the HVP contributions), but it is closer to the experimental value $\Delta a_\mu = a_\mu^{\text{exp}} - a_\mu^{\text{SM,LQCD}} = 10.7(6.9) \times 10^{-10}$. Lattice calculations are performed using QCD's fundamental degrees of freedom to evaluate the HVP contributions; the dispersive evaluations are built up from the sum of cross sections over exclusive hadronic channels to saturate the HVP in the nonperturbative low energy regime. While dispersive calculations of the HVP contributions using the same input data seem to largely agree among them [3–10,23,24], new independent and more precise lattice evaluations may confirm or discard the results of Ref. [27].

If more precise evaluations confirm the difference between lattice and dispersive $a_\mu^{\text{had,LO}}$ results, currently at the 2.1σ level, this will become another interesting anomaly to focus attention on theoretical predictions of a_μ . One possible explanation for closing the gap may be that some missing or poorly measured low-mass hadronic channels in electron-positron collisions contribute to increasing the value of the dispersive integral of the HVP. In this paper we study the contributions of the $P_1^0 P_2^0 \gamma$ processes ($P_{1,2} = \pi$ or η mesons) to the leading HVP contributions of the muon $g-2$ in the SM. These contributions are dominated by a rich structure of resonances with masses below 2 GeV. Actually, some of these resonance contributions like

*jlgutierrez@fis.cinvestav.mx

†glopez@fis.cinvestav.mx

Published by the American Physical Society under the terms of the Creative Commons Attribution 4.0 International license. Further distribution of this work must maintain attribution to the author(s) and the published article's title, journal citation, and DOI. Funded by SCOAP³.

$\omega\pi^0$, $\phi\eta$ and $\omega\eta$ (with the subsequent radiative decay of vector mesons) have been included in dispersive evaluations of the leading order HVP [8,9], using measurements of the $e^+e^- \rightarrow V^0P^0$ cross sections ($V(P)$ will refer hereafter to vector and pseudoscalar mesons). Other exclusive channels involving ω/ϕ resonances as final states have also been reported in dispersive evaluations of the $a_\mu^{\text{had,LO}}$ [8,9]. Some of the $e^+e^- \rightarrow P_1^0P_2^0\gamma$ channels have been studied before at lower energies, both from theory and experiment. Ref. [28] has used a dispersive approach to the $\pi^0\pi^0\gamma$ production and compared their results to measurements of the SND [29] and CMD-2 [30] collaborations. Reference [31] has studied the $(\pi^0\pi^0, \pi^0\eta)\gamma$ production close to the $\phi(1020)$ resonance including the effects of scalar $f_0(980)$ and $a_0(980)$ mesons in the hadronic system. The corresponding measurements of the $\phi(1020) \rightarrow \pi^0\eta\gamma$ decays by the KLOE collaboration were reported in [32,33]. These results from the KLOE experiment were also studied within the approach provided in Refs [34,35] where the $\gamma^* \rightarrow (\pi\eta, K\bar{K})\gamma$ amplitudes satisfy the two-channel unitarity. The effects of scalar resonances in $P_1^0P_2^0\gamma$ decays of light vector mesons also have been studied in Refs. [36–38]. In the vector meson model described in the present paper, we focus on the production of these neutral channels in the first and second excited resonances region, where the contribution to the HVP muon magnetic moment is larger than at lower energies.

Strictly speaking, according to the properties of the S -matrix, the amplitudes involving resonances as incoming/outgoing states are not physical observables [39,40]: only asymptotic physical states n (not resonances) must be included as intermediate states when saturating the unitarity relation:

$$2\text{Im}\langle\alpha|T|\alpha\rangle = \sum_n |\langle n|T|\alpha\rangle|^2 \quad (1)$$

that stems from the S -matrix operator, with $S = 1 + iT$ and $SS^\dagger = 11$. This unitarity relation is at the base of the dispersive representation of $a_\mu^{\text{had,LO}}$ and the hadronic cross sections of e^+e^- annihilations [41–43]. Therefore, from a theoretical point of view it is not fully consistent to use resonances as physical final states in hadronic e^+e^- cross sections, even though it can be a good approximation, particularly for very narrow resonances (see for instance Ref. [44]). This is the main motivation behind the present analysis on $P_1^0P_2^0\gamma$ exclusive channels contributions to $a_\mu^{\text{had,LO}}$.¹

¹Given their large lifetimes compared to hadrons that undergo dominant strong decays, π^0/η mesons can be considered asymptotic states.

The production cross section of $P_1^0P_2^0\gamma$ states are of the same order in the fine structure constant α as $P^0\gamma$ states, with the latter being included in evaluations of the HVP contribution ($a_\mu^{\text{had,LO}}(\pi^0\gamma + \eta\gamma) \simeq 5 \times 10^{-10}$ [8,9]). Note that the corresponding nonradiative $e^+e^- \rightarrow P_1^0P_2^0$ channels are not allowed final states, at least at leading order; therefore, $P_1^0P_2^0\gamma$ do not correspond to their photon inclusive processes. One may think that, given the low threshold for the $\pi^0\pi^0\gamma$ its contributions below the 1 GeV region may be enhanced due to the low energy behavior of the QED kernel in the dispersion integral for $a_\mu^{\text{had,LO}}$; however, as it will be shown, the cross sections for $P_1^0P_2^0\gamma$ production is peaked above 1 GeV, leading to suppressed contributions. This property follows from the particular Lorentz structure entering the $\gamma^* \rightarrow P_1^0P_2^0\gamma$ vertex which leads to e^+e^- cross sections peaked at center of mass energies above 1.4 GeV. Thus, when those cross sections are inserted into the dispersion integral to evaluate $a_\mu^{\text{had,LO}}$, the kernel suppression above 1 GeV can be partially compensated by the enhanced cross sections due to heavier resonances.

Previous calculations of $e^+e^- \rightarrow \pi^0\pi^0\gamma, \pi^0\eta\gamma$ cross sections in the region close to the $\phi(1020)$ meson have been provided in Refs. [31,35,45,46]. The corresponding cross section measurements were reported in [32,33,47], focusing mainly on the hadron mass distribution in $\phi \rightarrow P_1P_2\gamma$ decays. Measurements of the $e^+e^- \rightarrow \pi^0\eta\gamma$ cross section in the $\sqrt{s} = 1.05\text{--}2.0$ GeV region have been reported by the SND collaboration [48]. More recently, the first measurements of the $\eta\eta\gamma$ production cross section were reported in [49].

In the absence of experimental data (except for the $\pi^0\omega(\rightarrow \pi^0\gamma)$ channel [50,51]) in the full range below 2.0 GeV, we base our estimate on a vector meson dominance (VMD) model. This model captures the main features of the dynamics of such processes at energies around the resonance regions, and it can be validated with available data as is the case with the measured cross section for $e^+e^- \rightarrow \pi^0\pi^0\gamma$ [51]. Our purpose here is to describe the cross section in the region of the excited vector meson resonances, where an enhancement of the cross section can give a larger contribution to $a_\mu^{\text{had,LO}}$ from $P_1^0P_2^0\gamma$ states. A more sophisticated treatment of the $\gamma^* \rightarrow P_1^0P_2^0\gamma$ vertex can be done in the framework of resonance chiral theory by including the one- ($VP\gamma$) and two-resonances ($VV'P\gamma$) contributions. Although this analysis is possible, it involves a larger set of free parameters associated with the coupling of excited resonances. We do not consider this and other approaches in the present work. As previously mentioned, the description of $(\pi^0\pi^0, \pi^0\eta)\gamma$ production cross sections below 1 GeV, was studied in Refs. [28,34,35] using unitarity, analyticity, and low-energy constraints for the amplitudes. Here, we validate our VMD model by comparing it with some related measurements below 1 GeV.

We organize our paper as follows: after this introduction, we describe in Sec. II the general amplitude and relevant kinematics for the $e^+e^- \rightarrow P_1^0 P_2^0 \gamma$ collisions and introduce some useful notations. In Sec. III we derive the form factors for the vector-vector contributions to the hadronic vertex. Section III B considers the vector-scalar contributions in the special case of the $\gamma^* \rightarrow \pi^0 \eta \gamma$ vertex. In Sec. IV we use available data on the $e^+e^- \rightarrow \pi^0 \omega (\rightarrow \pi^0 \gamma)$ cross section to fit some of the parameters of the model and describe how the remaining parameters can be estimated from other data; we also provide our results for the cross sections of different channels. We use the calculated cross sections to compute the dispersive integral and get results for $a_\mu^{\text{had,LO}}(P_1^0 P_2^0 \gamma)$ in Sec. V. Finally, we give our conclusions in Sec. VI and include two relevant appendices.

II. AMPLITUDE AND KINEMATICS

In S-matrix theory, the quantum amplitudes describe transitions between incoming and outgoing stable states [39]. These initial and final states contain particles that must be described by asymptotic states, i.e., free particle states that can be defined at times long enough before and after the interaction point. According to this tenet of quantum scattering theory, resonances are not asymptotic states; instead, they are described by propagators of unstable particles and appear as poles of the amplitudes in the complex plane of unphysical sheets (see, for instance, the section on resonances in Ref. [22]). Physical states also form a complete set $\{|n\rangle\}$ which satisfy the unitarity condition $\sum_n |n\rangle\langle n| = 1$. The unitarity of the S-matrix operator ($S = 1 + iT$, where T is the transition operator) implies Eq. (1).

Similarly, the use of unitarity in the form of the optical theorem, which allows to relate the HVP of a_μ to the cross section for hadron production in electron-positron annihilation via a dispersion relation [41–43], requires that only asymptotic states are included in the final states of e^+e^- annihilations. Experiments have revealed that multihadron production processes are dominated by intermediate resonances which interfere in the squared amplitude. Owing to interference effects, we cannot isolate the observables associated with the production of a given resonance, although it can be a good approximation if the full transition probability is dominated by the production of that resonance [40,44]. One such example is precisely $e^+e^- \rightarrow \pi^0 \pi^0 \gamma$, where the intermediate state $\omega \rightarrow \pi^0 \gamma$ dominates the cross section.

In this paper, we study how the cross sections behave when one considers the full $e^+e^- \rightarrow P_1^0 P_2^0 \gamma$ processes including all resonances and their interference and we compare our results with the particular case where a single resonance contribution is assumed to dominate the cross section. Our purpose is to reevaluate the HVP contribution to a_μ by avoiding the use of resonances as final states.

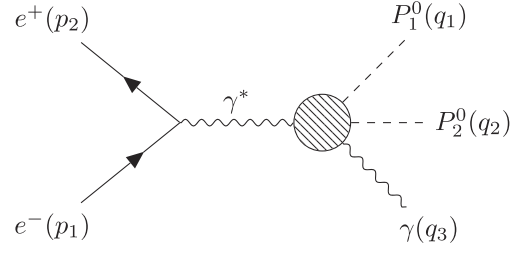


FIG. 1. Feynman diagram for $e^+e^- \rightarrow P_1^0 P_2^0 \gamma$, where $P_{1,2}^0 = \pi^0$ or η . The bubble represents the effects of strong interactions.

For definiteness, we introduce the notation $e^+(p_1)e^-(p_2) \rightarrow P_1^0(q_1)P_2^0(q_2)\gamma(q_3, \epsilon^*)$, with $p_1^2 = p_2^2 = m^2$, $q_1^2 = m_1^2$, $q_2^2 = m_2^2$, $q_3^2 = 0$ the masses of particles. The square of the center of mass energy is $s = q^2 = (p_1 + p_2)^2$, such that $s_{\text{min}} = (m_1 + m_2)^2 \gg 4m^2$. The final state can be characterized by three Mandelstam-like variables $q'^2 = (q_2 + q_3)^2$, $q''^2 = (q_1 + q_3)^2$ and $u = (q_1 + q_2)^2$, which satisfy the conditions $q'^2 + q''^2 + u = q^2 + m_1^2 + m_2^2$ and $q = q_1 + q_2 + q_3 = q' + q'' - q_3$ for the energy-momentum conservation.

At the lowest order in α , the Feynman diagram for this process is depicted in Fig. 1. The production amplitude can be presented in the following factorized form:

$$\mathcal{M}(e^+e^- \rightarrow P_1^0 P_2^0 \gamma) = -ie \frac{\ell^\mu}{q^2} H_\mu, \quad (2)$$

where $\ell^\mu = \bar{v}(p_2)\gamma^\mu u(p_1)$ is the leptonic current and $H_\mu = H_{\mu\sigma}\epsilon^{*\sigma} = \langle P_1^0 P_2^0 \gamma | j_\mu^{\text{em}} | 0 \rangle$ is the hadronic effective current and ϵ^* the photon polarization four-vector.

The most general form of the hadronic tensor $H_{\mu\sigma}$, which satisfies the gauge invariance conditions $q^\mu H_{\mu\sigma} = H_{\mu\sigma} q_3^\sigma = 0$ was given in Eqs. (4)–(7) of Ref. [28]. There, a clever set of independent momenta ($q, q_3, \Delta \equiv q_1 - q_2$), was used to describe $H_{\mu\sigma}$. Here, we use the redundant set (q, q', q'', q_3) because they are the “natural” momenta that appear in our calculations (see below) to parametrize the hadronic vertex. In this case, we have

$$\begin{aligned} H_{\mu\sigma} = & A(q \cdot q_3 g_{\mu\sigma} - q_{3\mu} q_\sigma) + B[q \cdot q' (q' \cdot q_3 g_{\mu\sigma} - q_{3\mu} q'_\sigma) \\ & - (q' \cdot q_3 q_\sigma - q \cdot q_3 q'_\sigma) q'_\mu] + C[q \cdot q'' (q'' \cdot q_3 g_{\mu\sigma} - q_{3\mu} q''_\sigma) \\ & - (q'' \cdot q_3 q_\sigma - q \cdot q_3 q''_\sigma) q''_\mu]. \end{aligned} \quad (3)$$

Of course, only three momenta are independent owing to the energy-momentum conservation $q = q' + q'' - q_3$. It can be shown that replacing $q' \rightarrow (q + q_3 - \Delta)/2$ and $q'' \rightarrow (q + q_3 + \Delta)/2$ into Eq. (3) above, we get for $H_{\mu\sigma}$ the same expression as the one given in Eqs. (4)–(7) of Ref. [28]. The form factors A, B, C depend upon the independent Lorentz invariants (q^2, q'^2, q''^2) and contain the effects of the strong interactions in the relevant kinematical domain.

The squared amplitude depends upon four independent kinematical invariants in addition to q^2 , which is fixed from the total collision energy. Since the $P_1^0 P_2^0 \gamma$ final states are produced from the s -channel one-photon annihilation of $e^+ e^-$, the cross section can be written in the following simple form (see for example [52])

$$\sigma(e^+ e^- \rightarrow P_1^0 P_2^0 \gamma) = \int_{m_2^2}^{(\sqrt{q^2} - m_1)^2} dq^2 \int_{q_+^{\prime 2}}^{q_+^{\prime 2}} dq^{\prime 2} \frac{d^2 \sigma}{dq^2 dq^{\prime 2}}, \quad (4)$$

where $q_{\pm}^{\prime 2} = (E_1^* + E_3^*)^2 - (\sqrt{E_1^{*2} - m_1^2} \mp E_3^*)^2$, with $E_1^* = (q^2 - q^{\prime 2} - m_1^2)/(2\sqrt{q^2})$ and $E_3^* = (q^2 - m_2^2)/(2\sqrt{q^2})$. The differential cross section in the integrand of Eq. (4) is given by

$$\frac{d^2 \sigma}{dq^2 dq^{\prime 2}} = \frac{\alpha}{48(2\pi)^2 q^6} |H_{\mu\sigma} H^{*\mu\sigma}|. \quad (5)$$

In the following section we consider the VMD model for the hadronic current.

III. FORM FACTORS WITHIN THE VMD MODEL

In the region $\sqrt{q^2} \leq 2$ GeV, the $\gamma^*(q) \rightarrow P_1^0(q_1) P_2^0(q_2) \gamma(q_3)$ vertex is dominated by the production and decay of lowest-lying and excited intermediate resonances. We will denote with $V(V')$ the intermediate vector resonances as shown in Fig. 2(a); within the VMD model, the coupling of the virtual photon to the $P_1^0 P_2^0 \gamma$ is dominated by the V vector meson ($V = \rho, \omega, \phi$ and their radial excitations). The final state is assumed to be dominated by either, the $P_i^0 V'$ ($i = 1, 2, V' = \rho, \omega, \phi$) or the $S\gamma$ intermediate states, with the subsequent radiative V' decay or the strong $S \rightarrow P_1^0 P_2^0$ decay of the scalar meson [see Fig. 2(b)]. Accordingly, we can decompose the hadronic tensor into two components $H_{\mu\sigma} = H_{\mu\sigma}^V + H_{\mu\sigma}^S$, where the superscripts V and S refer to the contributions of diagrams (a) and (b) in Fig. 2, respectively.

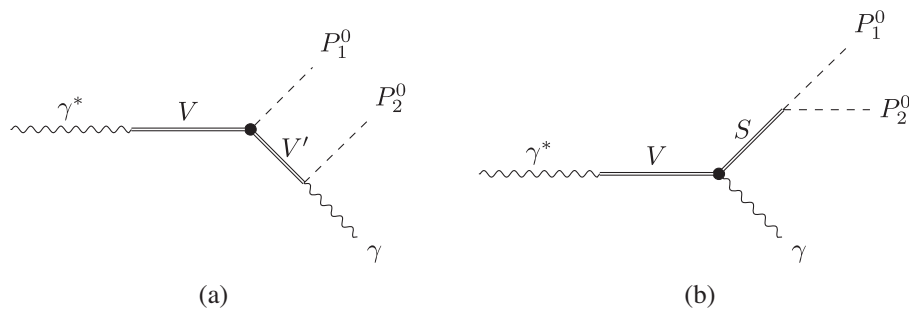


FIG. 2. Feynman diagrams describing the $\gamma^* \rightarrow P_1^0 P_2^0 \gamma$ vertex in a meson dominance model. Here V (and V') are intermediate vector meson resonances and S is a scalar meson. Diagrams with exchanged mesons in the final states for diagram (a) must be added to account for Bose statistics ($P_1^0 = P_2^0$) or allowed exchange contributions ($P_1^0 \neq P_2^0$).

A. Vector-vector contributions

The contributions to diagrams with two vector resonances in the VMD model are shown in Fig. 2(a). We need in this case to consider the $V(V')P\gamma$ and $VV'P$ interaction Lagrangians. The phenomenological Lagrangian density required to describe the $VP\gamma$ vertices is given by [53]

$$\mathcal{L}_{VP\gamma} = g\epsilon_{\mu\nu\alpha\beta} \partial^\mu A^\nu \text{Tr}[Q(\partial^\alpha V^\beta P + P\partial^\alpha V^\beta)]. \quad (6)$$

In this Lagrangian g is a generic coupling, A^μ is the photon field, $P(V^\beta)$ is the 3×3 matrix of light pseudoscalar (vector) mesons, and $Q = \text{diag}(2/3, -1/3, -1/3)$ is the matrix of light quark charges.

Also, one can include isospin and SU(3) breaking effects and try to extract, for lowest-lying mesons, the relevant parameters from a global fit to the available data on radiative meson decays, as done for example in Refs. [54] with effective couplings $g_{VP\gamma}$ (which is related to g defined in (6) for each specific channel [53,54]). The couplings $g_{VP\gamma}$ can be extracted from the measured rates of radiative meson decays [53,54]

$$\Gamma(V \rightarrow P\gamma) = \frac{1}{3} \Gamma(P \rightarrow V\gamma) = \frac{1}{12\pi} g_{VP\gamma}^2 |\vec{P}_\gamma|^3, \quad (7)$$

where $g_{VP\gamma}$ is the coupling for the specific $VP\gamma$ vertex and \vec{P}_γ the photon three-momentum in the decaying particle's rest frame in each specific decay. The values extracted from the radiative decays of light vector mesons are displayed in the lower part of Table I.

In addition, we need information on the $VV'P$ couplings of the radially excited vector mesons V (here V' is a light vector meson) and its couplings to photons that enter the $\gamma^* \rightarrow V \rightarrow V'P$ vertex. Individual measurements of the strong or lepton-pair decays of excited vector mesons needed to determine such couplings are not reported by the PDG [22]. However, some (model-dependent) analysis of experimental data, mainly from the SND [48,51,55,57], CMD-3 [56], BABAR [58], and BESIII [59] collaborations, allow to extract the ratio of relevant constants $g_{VV'P}/\gamma_V$,

TABLE I. Values of model-dependent coupling constants. Entries in the upper part refer to the values extracted from the peak cross sections of $e^+e^- \rightarrow V \rightarrow V'P$ as explained in the text using Eqs. (8), (20). Values of the middle part are extracted using the VMD expressions for $V \rightarrow P\gamma$ and $g_{VP\gamma}$ couplings (lower part of table) from Ref. [54].

Parameter	Transition	Value	Reference
$g_{VV'P}/\gamma_V$ [GeV ⁻¹]	$\rho(1450) \rightarrow \omega\pi^0$	0.5351 ± 0.0709	SND 2016 [51]
	$\rho(1700) \rightarrow \omega\pi^0$	0.0425 ± 0.0207	SND 2016 [51]
	$\omega(1420) \rightarrow \rho\pi^0$	0.6808 ± 0.1564	SND 2015 [55]
	$\omega(1650) \rightarrow \rho\pi^0$	0.2329 ± 0.0286	SND 2015 [55]
	$\omega(1420) \rightarrow \omega\eta$	0.1984 ± 0.1237	SND 2020 [48]
	$\omega(1650) \rightarrow \omega\eta$	0.0735 ± 0.0120	SND 2020 [48]
	$\rho(1450) \rightarrow \rho\eta$	0.5177 ± 0.0430	CMD-3 2020 [56]
	$\rho(1700) \rightarrow \rho\eta$	0.0048 ± 0.0013	CMD-3 2020 [56]
	$\phi(1680) \rightarrow \phi\eta$	0.2875 ± 0.0818	SND 2019 [57]
	$\phi(2170) \rightarrow \phi\eta$	0.0048 ± 0.0074	BABAR 2007 [58]
$g_{VV'P}/\gamma_V$ [GeV ⁻¹]	$\phi(2170) \rightarrow \omega\eta$	0.0027 ± 0.0006	BESIII 2020 [59]
	$\rho \rightarrow \rho\eta$	1.5181 ± 0.0234	
	$\phi \rightarrow \phi\eta$	0.6912 ± 0.0152	
$g_{VP\gamma}$ [GeV ⁻¹]	$\omega \rightarrow \omega\eta$	0.4580 ± 0.0287	
	$\rho \rightarrow \pi^0\gamma$	0.2441 ± 0.0071	[54]
	$\rho \rightarrow \eta\gamma$	0.4597 ± 0.0174	[54]
	$\omega \rightarrow \pi^0\gamma$	0.6935 ± 0.0104	[54]
	$\omega \rightarrow \eta\gamma$	0.1387 ± 0.0087	[54]
	$\phi \rightarrow \pi^0\gamma$	0.0410 ± 0.0037	[54]
	$\phi \rightarrow \eta\gamma$	0.2093 ± 0.0046	[54]

where V represents an excited vector meson and em_V^2/γ_V its coupling to virtual photons. This product of coupling constants can be extracted from measurements of the cross section at the peak of these V resonances which determines the product of their decay rates into $V'P$ and lepton pairs [22] through the expression

$$\sigma_{\text{peak}}(e^+e^- \rightarrow V'P) = \frac{12\pi}{m_V^2} \cdot \frac{\Gamma(V \rightarrow e^+e^-)\Gamma(V \rightarrow V'P)}{\Gamma_V^2}, \quad (8)$$

where $m_V(\Gamma_V)$ is the mass (width) of the intermediate s -channel resonances and $\Gamma(V \rightarrow X)$ their partial decay widths into the X channel. The values of the $X_{VV'P} \equiv g_{VV'P}/\gamma_V$ ratios extracted from Eqs. (8) and (20) are given in the upper part of Table I.

With the above ingredients, we can build the amplitude for VV' contributions of Fig. 2(a). The hadronic tensor corresponding to the specific configuration shown in that figure reads:

$$\begin{aligned} H_{\mu\sigma}^V &= F^{P_1 P_2 \gamma}(u, q^2, q'^2; q^2) \varepsilon_{\alpha\mu\beta} \varepsilon_{\lambda\sigma\omega}^{\alpha} q'^{\nu} q^{\beta} q'^{\lambda} q_3^{\omega} \\ &= F^{P_1 P_2 \gamma}(u, q^2, q'^2; q^2) \times \{ q'^2 [(q \cdot q_3) g^{\mu\sigma} - q_3^{\mu} q^{\sigma}] \\ &\quad - (q \cdot q') [(q' \cdot q_3) g^{\mu\sigma} - q_3^{\mu} q'^{\sigma}] + (q' \cdot q_3) q'^{\mu} q^{\sigma} \\ &\quad - (q \cdot q_3) q^{\mu} q'^{\sigma} \} + (q_1 \leftrightarrow q_2). \end{aligned} \quad (9)$$

Note that, the last term in Eq. (9) symmetrizes the amplitude for identical mesons in the final state ($\pi^0\pi^0, \eta\eta$), and

considers the case with exchanged $\pi^0 \leftrightarrow \eta$ in the $\pi\eta$ channel. In the case of identical mesons a $1/2!$ factor must be included in the phase space factor. In the above expression, the form factor $F^{P_1 P_2 \gamma}(u, q^2, q'^2; q^2)$ contains information on the production and decay of intermediate resonance states. As expected, the hadronic tensor for vector contributions has the structure derived in Eq. (3).

The squared amplitude for vector-vector contributions will be enhanced at higher c.m.s. energies owing to the Lorentz structure involving quartic momentum dependence of the hadronic vertex [see Eq. (9)]; in addition, this enhancement is further favored by the effects of radially excited s -channel resonances produced. Owing to this behavior we will include the light and first/second radially excited V resonances in the s -channel, but we keep only the contributions of the lightest vector V' resonances decaying into $(P_2^0, P_1^0)\gamma$ final states. Accordingly, we write the form factors for the three processes under consideration as follows (the variables q'^2, q''^2, u , and q^2 in the argument of the form factors are omitted):

$$F^{\pi^0\pi^0\gamma} = F_{\rho}^{\pi^0\pi^0\gamma} + F_{\omega}^{\pi^0\pi^0\gamma} + F_{\phi}^{\pi^0\pi^0\gamma}, \quad (10)$$

$$F^{\pi^0\eta\gamma} = F_{\rho}^{\pi^0\eta\gamma} + F_{\omega}^{\pi^0\eta\gamma} + F_{\phi}^{\pi^0\eta\gamma}, \quad (11)$$

$$F^{\eta\eta\gamma} = F_{\rho}^{\eta\eta\gamma} + F_{\omega}^{\eta\eta\gamma} + F_{\phi}^{\eta\eta\gamma}. \quad (12)$$

The subindices on the right-hand side refer to the light vector resonances V' decaying into $(P_2^0, P_1^0)\gamma$. An analogous

expression to Eq. (11), namely $F^{\eta\pi^0\gamma}$, must be taken into account for the exchange $\pi^0 \leftrightarrow \eta$ in the final state. The explicit expressions for each contribution are given in Appendix.

B. Vector-scalar contributions

In addition to VV' contributions discussed in the previous section, scalar resonances can contribute to $e^+e^- \rightarrow P_1^0 P_2^0 \gamma$ as shown in Fig. 2(b). Among the different final states studied in this paper, only the $a_0(980) \rightarrow \pi^0 \eta$ (and possibly its ‘‘excited’’ scalar state) and the $f_0(980) \rightarrow \pi^0 \pi^0$ can contribute sizably [32,33,35,47,48].

The hadronic tensor in this case has a simpler form:

$$H_{\mu\sigma}^S = ieS^{P_1 P_2 \gamma}(q^2, q'^2, u; q^2)(q \cdot q_3 g_{\mu\sigma} - q_{3\mu} q_\sigma). \quad (13)$$

This Lorentz structure agrees with the general parametrization given in Eq. (3).

According to Fig. 2(b), we need information about the $VS\gamma$ and $S\eta\pi$ interaction couplings. The vertex $VS\gamma$ responsible for the scalar resonance production is described by the Lagrangian $\mathcal{L} = (eg_{VS\gamma}/2)F^{\mu\nu}V_{\mu\nu}\phi_S$, where $(V, F)_{\mu\nu}$ are the field strength tensors of the vector-meson and photon, respectively, while ϕ_S denotes the field of the scalar meson. The Feynman rule describing the $SP_1 P_2$ vertex is given by $ig_{SP_1 P_2}$. The form factor describing the $\gamma^*(q) \rightarrow V(q) \rightarrow S(\rightarrow P_1^0 P_2^0)\gamma$ vertex is given by

$$S^{P_1 P_2 \gamma}(q^2, q'^2, u; q^2) = e \sum_V \frac{m_V^2}{\gamma_V D_V(q^2)} \sum_S g_{VS\gamma} \cdot \frac{g_{SP_1 P_2}}{D_S(u)}. \quad (14)$$

In the above expressions, $D_{V,S}(x) = m_{V,S}^2 - x - i\sqrt{x}\Gamma_{V,S}(x)$ denote the denominators of vector (V) and scalar (S) resonance propagators, while $\Gamma_i(x)$ denote their total decay widths at squared momentum x .

In the case of the $\pi^0 \pi^0$ channels, we can have the contributions of the isoscalar scalar $f_0(500)$ and $f_0(980)$ states; we will consider the effects of the latter as it is better established as a resonance [22]. For the $\pi^0 \eta$ channel, we will include the contributions of the isovector $a_0(980)$, $a_0(1450)$ (or a_0, a'_0 , respectively, for short) decaying (this expression agrees with Eq. (4.1) in Ref. [31] in the case of a single vector and scalar resonance).

One may attempt to extract the relevant couplings of scalar mesons from experimental data. Unfortunately, the experimental information on these decays is rather scarce, if not completely missing.² Therefore, we will proceed to use a combination of experimental information, theoretical

²The nature of scalar mesons and their classification is still controversial [22]. The resonance parameters and some relevant decay channels of the a'_0 are better known than those of the lightest a_0 meson. [22].

predictions and make the assumption that, in a specific energy region, only one vector resonance V in the s -channel dominates the scalar meson ($V \rightarrow S\gamma \rightarrow P_1 P_2 \gamma$) production to provide an estimate of their effects in the cross section:

1. We will assume that the dominant contribution to the $e^+e^- \rightarrow \pi^0 \eta \gamma$ cross section below $\sqrt{s} = 1.2$ GeV comes from the $\gamma^* \rightarrow \phi(1020) \rightarrow a_0(980)[\rightarrow \pi^0 \eta]\gamma$ transition, because both (ϕ and a_0) can be produced on their mass-shell. Therefore, we use the resonance parameters of the $a_0(980)$ scalar meson as determined in the analysis of the $\phi \rightarrow \pi^0 \eta \gamma$ hadronic mass distribution measured by KLOE [32] using the resonance model of Ref. [31], namely: $|g_{a_0 \eta \pi}| = 2.46(14)$ GeV and $m_{a_0} = 982.5$ MeV (fixed), $\Gamma_{a_0} = 80$ MeV. The coupling $g_{\phi a_0 \gamma} = 0.524(11)$ GeV⁻¹ is extracted from the measured branching fraction of $\phi \rightarrow a_0 \gamma$ [22].
2. The measured branching fraction of $a'_0(1450) \rightarrow \eta \pi$ is reported in [22]. Using the $\Gamma(a'_0 \rightarrow \eta \pi) = (g_{a'_0 \eta \pi}^2/8\pi) \cdot |\vec{p}_\pi|/m_{a'_0}^2$ decay rate we get $g_{a'_0 \eta \pi} = 1.46(16)$ GeV. The mass and width parameters of the a'_0 are taken from the PDG [22].
3. We will assume that, in the region of excited vector V resonances, only one of them dominates the $\gamma^* \rightarrow V \rightarrow a'_0 \gamma$ vertex. Further, we assume that this vector resonance is the excited state $\phi' = \phi(1680)$. From the following vector-meson dominance relations among the couplings (a similar relation holds for the $a_0 \gamma^* \gamma$ coupling)

$$g_{a'_0 \gamma^* \gamma}(q^2) = e \sum_V \frac{g_{a'_0 V \gamma}}{\gamma_V} \cdot \frac{m_V^2}{D_V(q^2)}, \quad (15)$$

and assuming the dominance of the $\phi'(1680)$, one gets at $q^2=0$, $g_{a'_0 \gamma \gamma} = eg_{a'_0 \phi' \gamma}/\gamma_{\phi'}$. Using the predicted rate for the $\Gamma_{a'_0 \gamma \gamma} = (g_{a'_0 \gamma \gamma}^2/4\pi)m_{a'_0}^3 = 1.05(5)$ keV [34], we get $g_{a'_0 \phi' \gamma}/\gamma_{\phi'} = 0.0067(2)$ GeV⁻¹ from the above VMD relation.³

4. There are two possible isoscalar scalar mesons that can mediate the $\pi^0 \pi^0$ system: the $f_0(500)$ and the $f_0(980)$ below the 1.2 GeV region. As in the previous case, we assume their contribution will be larger when both, the vector resonance in the s -channel and the scalar resonances can be on-shell. The dominant contribution comes from the $\gamma^* \rightarrow \phi(1020) \rightarrow f_0(980)[\rightarrow \pi^0 \pi^0]\gamma$ decay chain. We use the resonance parameters of the $f_0(980)$ scalar meson as determined in the analysis of the $\phi \rightarrow \pi^0 \pi^0 \gamma$ hadronic mass distribution measured by KLOE [60]:

³Note that our $g_{a'_0 \gamma \gamma}$ and the one $\tilde{g}_{a'_0 \gamma \gamma}$ used in Ref. [34], are related by $g_{a'_0 \gamma \gamma} m_{a'_0}^2 = \tilde{g}_{a'_0 \gamma \gamma}/2$.

$|g_{f_0\pi^0\pi^0}| = 0.926(64)$ GeV and $m_{f_0} = (984.7 \pm 0.4^{+2.4}_{-3.7})$ MeV (the first error is from the fit and the second one has a systematic nature), and an energy-dependent width of the $f_0(980)$ is assumed [60]. We also use $g_{\phi f_0\gamma} = (2.61 \pm 0.02^{+0.31}_{-0.08})$ GeV⁻¹ [60].

- Some evidence has been reported for the lighter isoscalar meson in $(\rho^0, \omega) \rightarrow f_0(500)[\rightarrow \pi^0\pi^0]\gamma$ transitions (see [22] and references therein). Direct experimental information on its parameters and partial widths is scarce and indicates that $f_0(500)$ is a broad state, which is rather difficult to describe as a resonance with a Breit-Wigner propagator. Although the existence of this state is better established nowadays [61,62], we do not include it in our analysis because information on relevant couplings is missing. We expect its contribution to $a_\mu^{\text{had,LO}}(\pi^0\pi^0\gamma)$ to be small and covered by the quoted uncertainties of the dominant $\omega(\rightarrow\pi^0\gamma)\pi^0$ term.

Given all the approximations contained in the derivation of scalar couplings, we must take the predicted effects of scalar mesons in the cross section and $a_\mu^{\text{had,LO}}(\pi^0\eta\gamma)$ as an indication of their real size.

IV. CROSS SECTIONS FOR $P_1^0 P_2^0 \gamma$ CHANNELS

In this section, we consider separately the cross sections for the $e^+e^- \rightarrow (\pi^0\pi^0, \pi^0\eta, \eta\eta)\gamma$ reactions. We focus first, in more detail, on the $\pi^0\pi^0\gamma$ channel in order to fix some of the parameters of the model by comparing it with available data; this is the channel with the largest cross section among $P_1^0 P_2^0 \gamma$ final states owing to the large branching ratio for the $\omega \rightarrow \pi^0\gamma$ decay. Thereafter we consider the predictions for the other two channels. We do not expect our model to give a good description of the low-energy data. However, we compare our model with the cross section for $\pi^0\pi^0\gamma$ production below 1 GeV, and with the data on the di-photon spectrum in $\eta \rightarrow \pi^0\gamma\gamma$ decay as a validation of our model at lower energies.

A. $\pi^0\pi^0\gamma$ final state

Different experiments have reported measurements of the $e^+e^- \rightarrow \pi^0\pi^0\gamma$ cross section below 2 GeV. In the energy region below 1 GeV, the measurements of $\pi^0\pi^0\gamma$ production have been reported in references [29,30]. Above 1 GeV, the SND collaboration has provided results in the energy range $\sqrt{s} = 1.05\text{--}2.0$ GeV [50] and $\sqrt{s} = 1.047\text{--}2.005$ GeV [51], while the CMD-2 collaboration in the energy domain 1.380–0.920 GeV and DM2 [63] in the energy range from 1.350–2.4 GeV. The latter experiments focus on final states where the $\pi^0\gamma$ system originates from the $\omega(782)$ meson decays which, according to the present discussion, is one contribution to the full S-matrix amplitude for the $\pi^0\pi^0\gamma$ final state. In the VMD model, the different contributions with intermediate resonances are given by $e^+e^- \rightarrow V \rightarrow \pi^0(\rho, \omega, \phi) \rightarrow \pi^0\pi^0\gamma$. Accordingly, the general form of the

hadronic tensor was given in Eq. (9) with the specific invariant form factor

$$F^{\pi^0\pi^0\gamma}(u, q'^2, q''^2; q^2) = F_\rho^{\pi^0\pi^0\gamma} + F_\omega^{\pi^0\pi^0\gamma} + F_\phi^{\pi^0\pi^0\gamma}. \quad (16)$$

The explicit expressions for the different terms are given in Appendix. Dependence upon the same invariant variables must be understood for each term on the right-hand side of the above equation.

For the denominators of excited resonances' propagators in Eqs. (16) and (A1) we use Breit-Wigner forms with constant widths, namely $D_V(s) = m_V^2 - s - im_V\Gamma_V$, where $m_V(\Gamma_V)$ denote the mass (width) of resonances. The same consideration applies to the narrow (ω, ϕ) light meson resonances. However, following the SND collaboration [50,51] (and our own efforts to achieve a good fit), we use the following expression for the energy-dependent width of the $\rho(770)$ meson propagator $D_\rho(s) = m_\rho^2 - s - im_\rho\Gamma_\rho(s)$:

$$\Gamma_\rho(s) = \Gamma_{\rho\rightarrow\pi\pi}(s)\theta(\sqrt{s} - 2m_\pi) + \Gamma_{\rho\rightarrow\omega\pi}(s)\theta(\sqrt{s} - m_\omega - m_\pi), \quad (17)$$

where the energy-dependent partial widths are

$$\Gamma_{\rho\rightarrow\pi\pi}(s) = \Gamma_\rho \frac{m_\rho^2}{s} \left(\frac{s - 4m_\pi^2}{m_\rho^2 - 4m_\pi^2} \right)^{3/2}, \quad (18)$$

$$\Gamma_{V\rightarrow V'P} = \frac{g_{VV'P}^2}{96\pi} \left(\frac{\lambda(s, m_{V'}^2, m_P^2)}{s} \right)^{3/2} \quad (19)$$

with $\theta(x)$ and $\lambda(x, y, z)$ are the step and Kallen functions, respectively. Although Eq. (17) may look unusual, the opening of new thresholds (like $\omega\pi, K\bar{K}, \dots$) must be included in the decay width as the invariant mass of the resonance increases.⁴

The form factors given in Appendix depend upon several parameters: (a) the couplings $g_{VP\gamma}$ needed to describe $(\rho, \omega, \phi) \rightarrow P'\gamma$ decays in the sequence $V \rightarrow PV' \rightarrow PP'\gamma$ are taken from the fits of Ref. [54], and are listed in the lower part of Table I; (b) the ratio of couplings $X_{VV'P} \equiv g_{VV'P}/\gamma_V$ shown in the upper part of Table I were extracted from experimental values of the peak cross sections (8) using the theoretical expression

$$\frac{\Gamma_{V\rightarrow e^+e^-}\Gamma_{V\rightarrow V'P}}{\Gamma_V^2} = \frac{X_{VV'P}^2\alpha^2}{72} \cdot \frac{\lambda^{3/2}(m_V^2, m_{V'}^2, m_P^2)}{m_V^2\Gamma_V^2}; \quad (20)$$

(c) the strong $VV'\eta$ couplings for light resonances quoted in the middle part of Table I were extracted by combining the $g_{V\eta\gamma}$ couplings obtained in [54] and the em_V/γ_V couplings

⁴The $K\bar{K}$ channel opens at $\sqrt{s} = 0.99$ GeV, however it remains smaller than 6% of the $\pi\pi$ contribution in the region below $\sqrt{s} = m_\rho + 2\Gamma_\rho$.

TABLE II. Results of our fit (third column) to the $e^+e^- \rightarrow \pi^0\omega(\rightarrow\pi^0\gamma)$ cross section data [51], compared to results of Ref. [51] and the PDG values [22]. The † symbol means that the parameter has been fixed to their PDG values in the fit.

Parameter	SND values [51]	This work	PDG values [22]
$m_{\rho(1450)}$ [MeV]	1510 ± 7	1510 ± 12	1465 ± 25
$\Gamma_{\rho(1450)}$ [MeV]	440 ± 40	420 ± 50	400 ± 60
$m_{\rho(1700)}$ [MeV]†	1720 ± 20	1720 ± 20	1720 ± 20
$\Gamma_{\rho(1700)}$ [MeV] †	250 ± 100	250 ± 100	250 ± 100
$g_{\rho\omega\pi}$ [GeV ⁻¹]	15.9 ± 0.4	17.5 ± 1.3	12.47
γ_{ρ}	4.98
$X_{\rho'\omega\pi}$	0.56 ± 0.05	0.51 ± 0.06	0.535 [51]
$X_{\rho''\omega\pi}$	0.044 ± 0.013	0.037 ± 0.012	0.0425 [51]
ϕ_1 [deg]	124 ± 17	114 ± 34	127 ± 12
ϕ_2 [deg]	-63 ± 21	-80 ± 18	...
$\chi^2/\text{n.d.f}$	0.97	0.86	...

for the $\gamma - V$ conversion extracted from measured [22] $\Gamma_{V \rightarrow e^+e^-} = (4\pi\alpha^2/3\gamma_V^2)m_V$ partial rates and; (d) the masses and decay widths of remaining radially excited vector resonances were taken from [22]. For light vector resonances $\rho/\omega/\phi$ we assume their masses and widths world averaged values [22]. In the case of the isovector $\rho' = \rho(1450)$ and

$\rho'' = \rho(1700)$ mesons we extract the resonance parameters from a fit to the data of the SND collaboration [51], by assuming their contributions to be complex relative to the lightest $\rho(770)$ vector resonance.

In order to be more explicit, we rewrite the dominant contribution in Eq. (16) as follows:

$$F_{\omega\pi^0\gamma}^{\pi^0\pi^0\gamma} = ieX_{\rho\omega\pi} \left\{ \frac{m_{\rho}^2}{D_{\rho}(q^2)} + \frac{X_{\rho'\omega\pi}e^{i\phi_1}}{X_{\rho\omega\pi}} \frac{m_{\rho'}^2}{D_{\rho'}(q^2)} + \frac{X_{\rho''\omega\pi}e^{i\phi_2}}{X_{\rho\omega\pi}} \frac{m_{\rho''}^2}{D_{\rho''}(q^2)} \right\} \frac{g_{\omega\pi^0\gamma}}{D_{\omega}(q^2)}, \quad (21)$$

where X_V are taken to be real, since the relative phases are given explicitly. The $\rho(770)$ meson propagator $D_{\rho}(q^2)$ with the energy-dependent width is given in Eq. (17).

We can evaluate the cross section using the full S-matrix amplitude by inserting the form factors into Eq. (9), taking into account Bose symmetrization terms, and using Eq. (4) for the cross section. In order to compare to available data from SND [51] on the $e^+e^- \rightarrow \pi^0\omega(\rightarrow\pi^0\gamma)$ cross section in the $\sqrt{q^2} = 1.05\text{--}2.0$ GeV region,⁵ we turn off the first and last terms in Eq. (16). We let as free parameters: the resonance parameters of the $\rho(1450)$, the complex parameters $X_{\rho'\omega\pi}, X_{\rho''\omega\pi}$ (phases ϕ_1, ϕ_2 , respectively), and the $g_{\rho\omega\pi}$ coupling. The third column in Table II collects results of our fit to the cross section data of Ref. [51].

A comparison of the second and third columns in the same Table shows a good agreement between our results and those reported by the SND collaboration [51]. Our fit to the experimental data is shown with a dashed line in Fig. 3. In the same figure, we include (solid blue line) the cross section for $\pi^0\pi^0\gamma$ production by taking into account all terms in Eq. (16); except for the narrow peaks at the $\rho(770)$ (suppressed) and at the $\phi(1020)$ (more prominent)

resonance positions, the full and ω -dominance contributions agree in all the kinematical range under consideration.

References [29,30] have reported measurements of the $\pi^0\pi^0\gamma$ cross section at lower energies, in the center of mass energy $\sqrt{s} \sim 600\text{--}970$ MeV. Our model, extrapolated at these energies, is compared to these data in Fig. 4. The curve predicted by our model lies below the experimental data and the fit of Ref. [28], in the region of the $\rho(770)$ resonance but they agree reasonably well outside the resonance domain. A more quantitative comparison can be achieved by evaluating the $\hat{\chi}^2 = (1/N) \sum_i (\sigma_i^{\text{exp}} - \sigma_i^{\text{Model}})^2 / (\Delta\sigma_i)^2$ function, where N is the number of experimental data points in each dataset and $\Delta\sigma_i$, the quadrature of model and experimental uncertainties for the i th data point. We get $\hat{\chi}^2 = 1.13$ for the dataset of Ref. [29] dataset; $\hat{\chi}^2 = 1.01$ for Ref. [30], and $\hat{\chi}^2 = 1.54$ for the combination of both datasets. Our model is not optimal in this region, but given the large experimental errors, the value of $\hat{\chi}^2$ is reasonably good so far.

B. $\pi^0\eta\gamma$ final state

The amplitude corresponding to VV' contributions [Fig. 2(a)] for $e^+e^- \rightarrow \pi^0\eta\gamma$ must be added with the diagram arising from the exchange of π^0 and η mesons in the final state. Note, however, that the intermediate resonances V and V' must be chosen to conserve strong

⁵We use this dataset because it covers most of the range of center of mass energies. It is the only reason to avoid including data from CMD2 and DM2 collaborations.

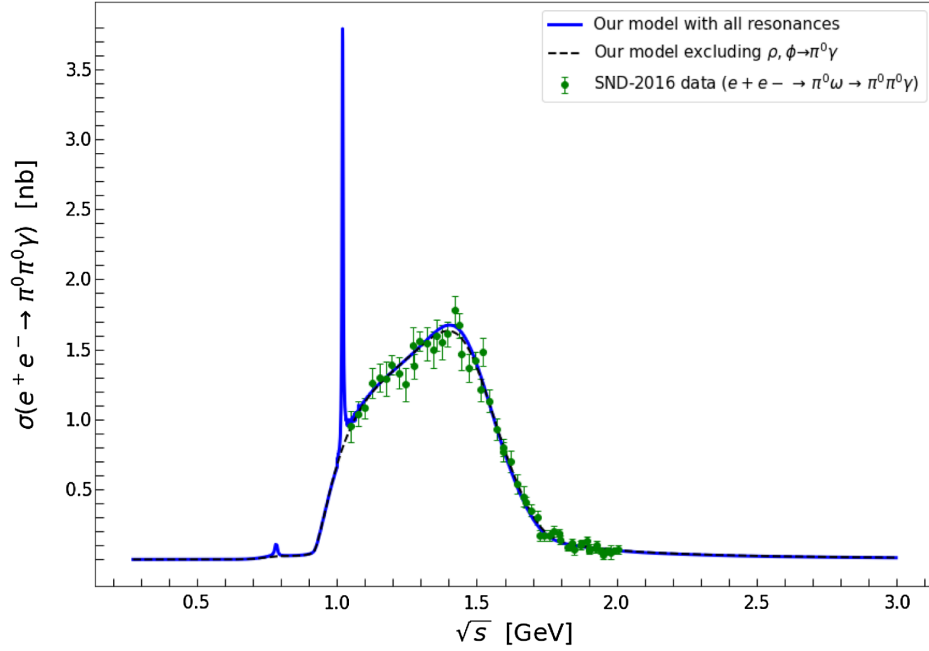


FIG. 3. Cross section for the $e^+e^- \rightarrow \pi^0\pi^0\gamma$ process. The solid line includes all the resonance contributions in Eq. (16). The dashed line corresponds to the dominance of the $\omega \rightarrow \pi^0\gamma$ decay, the second term in (16). The data points correspond to $e^+e^- \rightarrow \pi^0\omega(\rightarrow\pi^0\gamma)$ measured by SND [51].

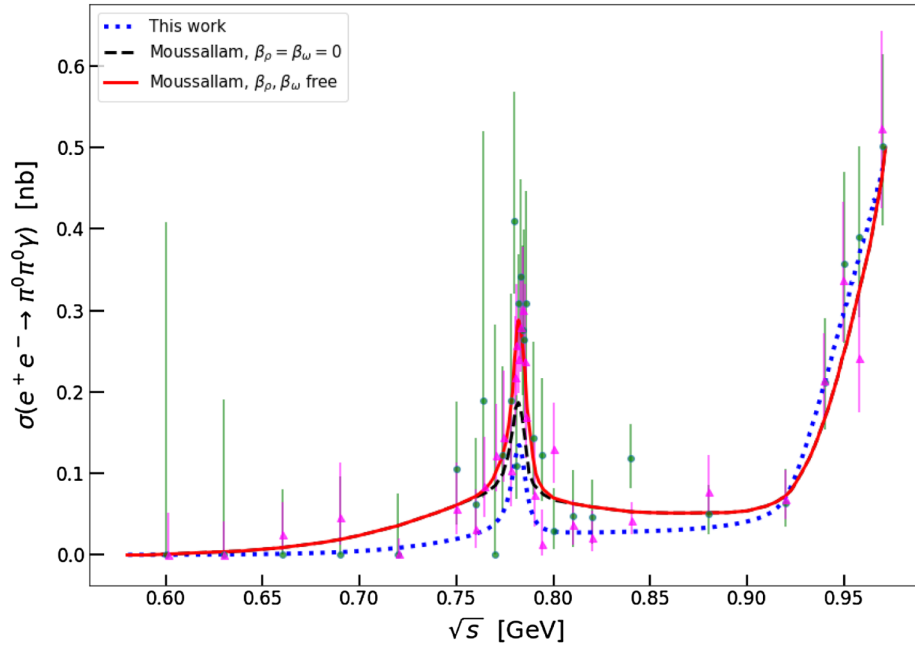


FIG. 4. Cross section for the $e^+e^- \rightarrow \pi^0\pi^0\gamma$ process below $\sqrt{s} = 0.97$ GeV. The dotted line corresponds to the VMD model used in this work. The dashed (solid) line corresponds to the fit of the model of Ref. [28] with (non)vanishing parameters β_ρ, β_ω to a combined dataset of SND [29] (triangles) and CMD-2 [30] (bullets) collaborations.

interaction symmetries in the $V \rightarrow \eta V'$ and $V \rightarrow \pi^0 V'$ vertices. Since this exchange contribution does not correspond to the exchange of identical particles in the final states, we do not have to add a $1/2!$ factor in the phase space.

As it was discussed in Sec. III B, contributions mediated by scalar mesons can appear in the $\pi^0\eta$ system through the $e^+e^- \rightarrow \gamma S(\rightarrow\eta\pi)$ mechanism ($S = a_0, a'_0$). Unfortunately, the situation concerning the experimental information on decay properties of the $a_0(=a_0(980))$ resonance and its

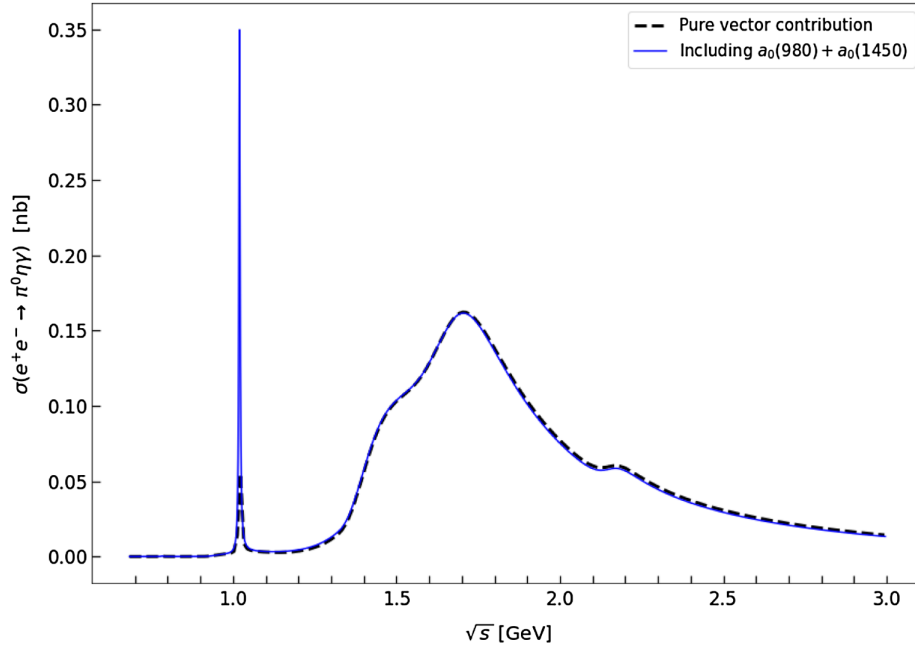


FIG. 5. Cross section for the $e^+e^- \rightarrow \pi^0\eta\gamma$ process. The dashed line corresponds to the pure $(V, V') = (1^{--}, 1^{--})$ contributions. The solid line includes, in addition, the effects of the $a_0(980)$ and $a'_0(1450)$ scalar mesons.

nature as a $q\bar{q}$, as tetraquark or as a molecular state is not very clear so far [22,64–67]. In contrast, the corresponding information for the $a'_0(=a_0(1450))$ properties is better known [22].

Despite these limitations, we have attempted an estimate of the effects of scalar resonances. We assume that the dominant contribution is given by the $\gamma^* \rightarrow \phi(1020) \rightarrow a_0\gamma$ chain contribution. Similarly, we assume that the $a'_0 = a_0(1450)$ production is dominated by $\gamma^* \rightarrow \phi'(1680) \rightarrow a'_0\gamma$. Our assumptions are based on the fact that at these center of mass energies, both the (ϕ, ϕ') vector and the (a_0, a'_0) scalar resonances can be produced on-shell, giving the largest contributions to the cross sections. Values of the coupling constants required in the model were described in Sec. III B. Of course, it corresponds to experiments to resolve the resonant structures present in the $\eta\pi^0$ and s -channels in the energy region under consideration.

The cross section plots are given in Fig. 5 as a function of the center of mass energy. The continuous line represents the sum of all the contributions, while the dashed line corresponds to the pure vector-vector (V, V') contributions. The sharp peak observed to the left is the effect of the ϕ meson decaying into the $a_0(980)$ meson and a photon; since the ϕ is a very narrow resonance, its contribution to $a_\mu^{\text{had,LO}}(\pi^0\eta\gamma)$ is subdominant. On the other hand, the effects of the $a_0(1450)$ scalar meson will be suppressed in $a_\mu^{\text{had,LO}}$ given the falling of the QED kernel in the dispersive relation.

The VMD for the $\pi^0\eta\gamma$ production channel can be compared to lower energy data of the crossed reactions $\gamma\gamma \rightarrow \pi^0\eta$ or $\eta \rightarrow \pi^0\gamma\gamma$. In the case of the latter decay, both

photons are real and a different kinematical region is tested, which lies well below the resonance region under consideration in this paper. In Fig. 6 the diphoton spectrum of $\eta \rightarrow \pi^0\gamma\gamma$ decays predicted in the VMD model of this work is compared to experimental data of Refs. [68,69]. Our prediction lies below data in the intermediate diphoton mass region.

By integrating over the full phase space, we get the following predictions for the partial decay width:

$$\begin{aligned} \Gamma(\eta \rightarrow \pi^0\gamma\gamma) &= \begin{cases} 0.216 \pm 0.021 \text{ eV}, & \text{for } V, V' \text{ contribs.} \\ 0.225 \pm 0.021 \text{ eV}, & \text{for } V, V' + a_0 + a'_0 \text{ contribs.} \end{cases} \end{aligned} \quad (22)$$

This result can be compared to the prediction of Ref. [34] $\Gamma(\eta \rightarrow \pi^0\gamma\gamma) = (0.237_{-0.043}^{+0.060})$ eV, and the current experimental value reported by the Particle Data Group $\Gamma(\eta \rightarrow \pi^0\gamma\gamma) = (0.334 \pm 0.032)$ eV [22].

C. $\eta\eta\gamma$ final state

The threshold energy for the $e^+e^- \rightarrow \eta\eta\gamma$ is $\sqrt{s} \approx 1.096$ GeV, well above the region of light vector resonances in the s -channel. The form factors for this final state are given in Eq. (12) and (A1), and the hadronic tensor (9) must include a symmetrization term according to Bose statistics. Using the input couplings shown in Table I, and the convention for the propagators discussed in previous sections, we evaluate the cross section using Eq. (4).

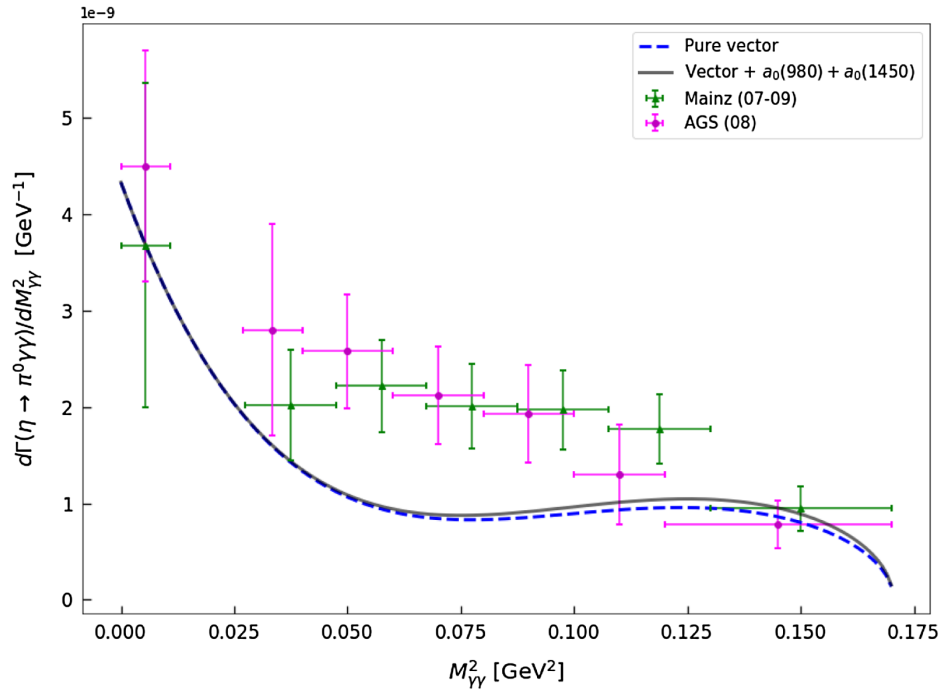


FIG. 6. The prediction of the VDM in this work is compared to experimental data of Refs. [68,69] on the diphoton spectrum of $\eta \rightarrow \pi^0\gamma\gamma$ decays. The dashed line corresponds to the pure vector contributions, whereas the solid line corresponds to the vector and scalar $a_0(980) + a_0(1450)$ contributions.

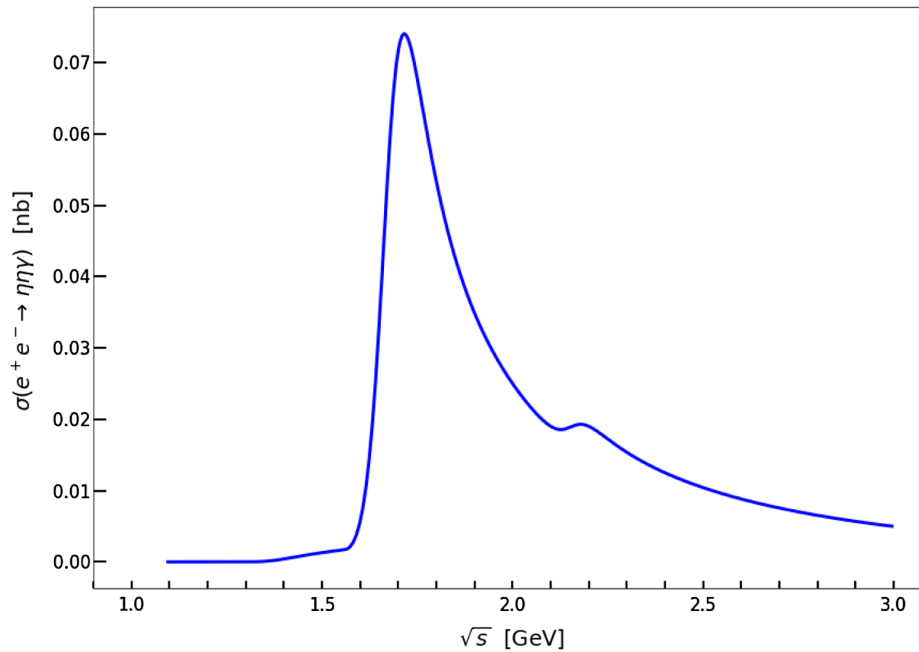


FIG. 7. Cross section for the $e^+e^- \rightarrow \eta\eta\gamma$ process. We use the VMD parameters reported in Table I.

In Fig. 7 we plot the $e^+e^- \rightarrow \eta\eta\gamma$ cross section from threshold up to 3.0 GeV. In the absence of experimental information on this decay channel, we assume the different contributions to add coherently with real and positive couplings between different resonance

contributions.⁶ A dominant peak is observed due to the $\rho(1700)$, and a smaller peak is barely visible at the $\phi(2170)$

⁶Given that $\eta\eta\gamma$ contribution to $a_\mu^{\text{had,LO}}$ is at the level of 10^{-12} , for now we can keep this approximation as safe.

resonance position. As expected, the cross section for $\eta\eta\gamma$ is smaller than the one due to $\pi^0\pi^0\gamma$ and $\pi^0\eta\gamma$.

V. $P_1^0 P_2^0 \gamma$ CONTRIBUTIONS TO a_μ

The HVP contributions to a_μ due to $e^+e^- \rightarrow P_1^0 P_2^0 \gamma$ processes can be written as follows [70,71]

$$a_\mu^{\text{had,LO}}(P_1^0 P_2^0 \gamma) = \left(\frac{\alpha}{3\pi}\right)^2 \int_{(m_1+m_2)^2}^{\infty} ds \frac{K(s) \sigma(e^+e^- \rightarrow P_1^0 P_2^0 \gamma)}{s \sigma_{\text{pt}}}, \quad (23)$$

where σ_{pt} is the point cross section for muon-pair production and $K(s)$ is the QED kernel that can be found, for instance, in Ref. [3].

If we insert the cross sections evaluated in this work into Eq. (23), we get the values shown in the second column of Table III. The second of the two results indicated for the $\pi^0\eta\gamma$ contribution corresponds to the inclusion of scalar resonances in this channel. The quoted errors stem from the uncertainties in couplings, masses and widths of vector and scalar intermediate resonances involved in each exclusive channel. Our largest uncertainty appears in the $\pi^0\pi^0\gamma$ contribution; it arises mainly from the uncertainties in the fitted $\rho'\omega\pi$ coupling quoted in Table II [22]. Since we do not use the dataset of all $e^+e^- \rightarrow \pi^0\omega(\rightarrow\pi^0\gamma)$ experimental cross sections, our quoted uncertainty for the $a_\mu^{\text{had,LO}}(\pi^0\pi^0\gamma)$ channel basically turns out to be larger than the ones quoted by references [8,9] (see discussion below).

We can attempt to make a (risky) comparison with Refs. [8,9], who have provided the evaluations of the $\pi^0\omega(\omega \rightarrow \pi^0\gamma)$, $\eta\omega$, and $\eta\phi$ contributions. For the values of $a_\mu^{\text{had,LO}}$ for the latter two channels provided in Refs. [8,9], we add the subsequent decays of (ω, ϕ) mesons into $(\pi^0, \eta)\gamma$ decays, which is justified in Appendix A. Under these assumptions, we can estimate the $P_1^0 P_2^0 \gamma$ contributions as follows ($B(X)$ denotes the branching fraction for channel X):

$$\begin{aligned} a_\mu(\pi^0\eta\gamma) &\simeq a_\mu(\eta\omega) \cdot B(\omega \rightarrow \pi^0\gamma) + a_\mu(\eta\phi) \cdot B(\phi \rightarrow \pi^0\gamma), \\ a_\mu(\eta\eta\gamma) &\simeq a_\mu(\eta\omega) \cdot B(\omega \rightarrow \eta\gamma) + a_\mu(\eta\phi) \cdot B(\phi \rightarrow \eta\gamma). \end{aligned} \quad (24)$$

Clearly, this represents, at most, an approximation to the complete evaluation. We use the values $a_\mu^{\text{had,LO}}(\eta\omega) = 0.35(1)(1)[0.30(2)]$ and $a_\mu^{\text{had,LO}}(\eta\phi) = 0.33(1)(1)[0.41(2)]$ from Ref. [8] (values obtained in [9] are indicated within square brackets), all numbers in 10^{-10} units, and the branching ratios reported in [22] for the radiative decays of vector mesons.

In columns fourth and fifth of Table III we write the values “estimated” following the above procedure. These values are underestimated with respect to our results and, in the case of the $\eta\eta\gamma$ channel, by almost one order of magnitude. It is expected since $\rho\eta$ and $\rho\pi^0$ exclusive channels are not reported separately and Eqs. (24) neglect interferences.

The contribution of the $\pi^0\pi^0\gamma$ channel to $a_\mu^{\text{had,LO}}$ in the energy region below $\sqrt{s} = 0.95$ GeV reported in [28] is $a_\mu^{\text{had,LO}}(\pi^0\pi^0\gamma) = 0.033(5) \times 10^{-10}$. Our corresponding contribution in the same interval is lower $0.020(3) \times 10^{-10}$, as it is expected from Fig. 4. The effects of the scalar resonances to $a_\mu^{\text{had,LO}}(P_1^0 P_2^0 \gamma)$ is roughly 4% of the total contributions, well within the quoted uncertainties of the dominant channel.

VI. CONCLUSIONS

In this paper we have considered the contributions of the neutral $e^+e^- \rightarrow \pi^0\pi^0\gamma, \pi^0\eta\gamma$ and $\eta\eta\gamma$ exclusive channels to the leading order HVP contributions of the muon anomalous magnetic moment. We evaluate these contributions by considering the full S-matrix amplitude for transitions between these asymptotic states, without cutting intermediate resonances. These decays are not the photon-inclusive

TABLE III. Contributions of $X = P_1 P_0 \gamma$ exclusive channels to $a_\mu^{\text{had,LO}}$ (in 10^{-10} units). The results of this work are given in the third column. Columns fourth and fifth for the $(\pi^0\eta, \eta\eta)\gamma$ contributions refer to the values estimated according to Eqs. (24) from the values of $\eta\omega$ and $\eta\phi$ contributions reported in Refs. [8,9], respectively. The effects of scalar (f_0, a_0, a'_0) mesons are shown separately.

X Channel	Contributions	$a_\mu^{\text{had,LO}}(X) \times 10^{-10}$		
		This work	DHMZ [8]	KNT [9]
$\pi^0\pi^0\gamma$	(V, V')	$1.002^{+0.129}_{-0.136}$	0.94(1)(3)	0.88(2)
$\pi^0\pi^0\gamma$	$(V, V') + f_0(980)$	$1.041^{+0.128}_{-0.137}$		
$\pi^0\eta\gamma$	(V, V')	$0.086^{+0.002}_{-0.001}$	0.030(2)	0.026(2)
$\pi^0\eta\gamma$	$(V, V') + a_0 + a'_0$	0.087 ± 0.001		
$\eta\eta\gamma$	(V, V')	$0.043^{+0.001}_{-0.002}$	0.0045(2)	0.0055(3)
	(V, V')	$1.131^{+0.129}_{-0.136}$		
Sum	$(V, V') + a_0 + a'_0 + f_0(980)$	$1.171^{+0.128}_{-0.137}$		

channels of $e^+e^- \rightarrow P_1^0 P_2^0$, $P_{1,2} = \eta$ or π , because such transitions are not allowed (at least at the lowest order in α) and are expected to be of the same order in α as the $\pi^0\gamma$ and $\eta\gamma$ channels. As it is well known [8,9], the latter contribute close to 1% to the total contributions of $a_\mu^{\text{had,LO}}$.

We describe the $\gamma^* \rightarrow P_1^0 P_2^0 \gamma$ vertex in the framework of vector meson dominance model. We validate this particular model by fitting the available data on the $e^+e^- \rightarrow \pi^0\omega(\omega \rightarrow \pi^0\gamma)$ channel; we also compared the predictions of our model to low energy data of the $e^+e^- \rightarrow \pi^0\pi^0\gamma$ cross section, and to the measured diphoton spectrum and the partial width of $\eta \rightarrow \pi^0\gamma\gamma$ decay. From the calculated cross sections we evaluate the corresponding dispersion integral and get the following prediction:

$$a_\mu^{\text{had,LO}}(\pi^0\pi^0\gamma + \pi^0\eta\gamma + \eta\eta\gamma) = (1.17^{+0.13}_{-0.14}) \times 10^{-10}.$$

The $\pi^0\pi^0\gamma$ exclusive channel dominates this result; this is in reasonable good agreement with the evaluation of Refs. [8,9] for the $\pi^0\omega(\omega \rightarrow \pi^0\gamma)$, where a comparison is possible. The other two contributions are more suppressed and a comparison with existing calculations is not straightforward. Our quoted uncertainty is dominated by errors in the strength coupling of the $\rho' \rightarrow \pi^0\pi^0\gamma$ decay within the VMD model and the particular dataset of $e^+e^- \rightarrow \pi^0\omega(\rightarrow\pi^0\gamma)$ measurements [51] used in our analysis.

The cross sections for $P_1^0 P_2^0 \gamma$ production are peaked in the region populated by excited vector resonances in the s -channel. It introduces important uncertainties in the calculation as long as the information on the parameters and decay properties of excited resonances are rather scarce or not very well known. In order to avoid all the uncertainties related to a particular model, it would be necessary to have better experimental data for these $P_1^0 P_2^0 \gamma$ final states in electron-positron collisions in the region below 2 GeV.

Of course, the dispersive calculation of $a_\mu^{\text{had,LO}}(P_1^0 P_2^0 \gamma)$ presented in this paper does not contribute sizably to closing the gap with the measured [1,2] and the lattice calculations of Ref. [27]. We address the problem of using exclusive channels with resonances and using them as inputs in the evaluation of $a_\mu^{\text{had,LO}}$. Using the S-matrix formalism with asymptotic states is important to assess the size of approximations done when one considers resonances as on-shell states and neglects interference with other contributions to the amplitude. It may not be obvious that separating resonance and background contributions from measured observables, is just an approximation. The clearest example that shows that interference effects are important is frequently found in the PDG [22], where the sum over final states involving resonances sometimes exceeds the branching ratios for some specific channels (for example

$B(D^0 \rightarrow \pi^+\pi^-\pi^0) = (1.49 \pm 0.06)\%$ while $\sum_{i,j} B(D^0 \rightarrow (\rho^i(770)\pi^j)^0 \rightarrow \pi^+\pi^-\pi^0) = (1.91 \pm 0.05)\%$ [22]).

ACKNOWLEDGMENTS

We are thankful to Michel Davier and Zhiqing Zhang for valuable discussions and comments. We are grateful to Pablo Roig for comments and Jean Pestieau for discussions. The work of G. L. C. was supported by Ciencia de Frontera Conacyt (México) Project No. 428218 and PRODEP IDPTC 162336. J. L. G. S. is grateful to Conacyt for financial support through a Ph.D. scholarship.

APPENDIX: FORM FACTORS IN $P_1^0 P_2^0 \gamma$ TRANSITIONS

In this appendix we provide the expressions for the form factors that contribute to the $P_1^0 P_2^0 \gamma$ transitions as defined in Sec. III A

$$\begin{aligned} F_\rho^{\pi^0\pi^0\gamma} &= ie \sum_{V=\omega,\phi,\dots} \frac{g_{V\rho^0\pi^0}}{\gamma_V} \cdot \frac{m_V^2}{D_V(q^2)} \cdot \frac{g_{\rho^0\pi^0\gamma}}{D_\rho(q^2)} \\ F_\omega^{\pi^0\pi^0\gamma} &= ie \sum_{V=\rho,\rho',\dots} \frac{g_{V\omega\pi^0}}{\gamma_V} \cdot \frac{m_V^2}{D_V(q^2)} \cdot \frac{g_{\omega\pi^0\gamma}}{D_\omega(q^2)} \\ F_\phi^{\pi^0\pi^0\gamma} &= ie \sum_{V=\rho,\rho',\dots} \frac{g_{V\phi\pi^0}}{\gamma_V} \cdot \frac{m_V^2}{D_V(q^2)} \cdot \frac{g_{\phi\pi^0\gamma}}{D_\phi(q^2)} \\ F_\rho^{\pi^0\eta\gamma} &= ie \sum_{V=\omega,\phi,\dots} \frac{g_{V\rho^0\pi^0}}{\gamma_V} \cdot \frac{m_V^2}{D_V(q^2)} \cdot \frac{g_{\rho^0\eta\gamma}}{D_\rho(q^2)} \\ F_\omega^{\pi^0\eta\gamma} &= ie \sum_{V=\rho,\rho',\dots} \frac{g_{V\omega\pi^0}}{\gamma_V} \cdot \frac{m_V^2}{D_V(q^2)} \cdot \frac{g_{\omega\eta\gamma}}{D_\omega(q^2)} \\ F_\phi^{\pi^0\eta\gamma} &= ie \sum_{V=\rho,\rho',\dots} \frac{g_{V\phi\pi^0}}{\gamma_V} \cdot \frac{m_V^2}{D_V(q^2)} \cdot \frac{g_{\phi\eta\gamma}}{D_\phi(q^2)} \\ F_\rho^{\eta\pi^0\gamma} &= ie \sum_{V=\rho,\rho',\dots} \frac{g_{V\rho^0\eta}}{\gamma_V} \cdot \frac{m_V^2}{D_V(q^2)} \cdot \frac{g_{\rho^0\pi^0\gamma}}{D_\rho(q^2)} \\ F_\omega^{\eta\pi^0\gamma} &= ie \sum_{V=\omega,\phi,\dots} \frac{g_{V\omega\eta}}{\gamma_V} \cdot \frac{m_V^2}{D_V(q^2)} \cdot \frac{g_{\omega\pi^0\gamma}}{D_\omega(q^2)} \\ F_\phi^{\eta\pi^0\gamma} &= ie \sum_{V=\omega,\phi,\dots} \frac{g_{V\phi\eta}}{\gamma_V} \cdot \frac{m_V^2}{D_V(q^2)} \cdot \frac{g_{\phi\pi^0\gamma}}{D_\phi(q^2)} \\ F_\rho^{\eta\eta\gamma} &= ie \sum_{V=\rho,\rho',\rho'',\dots} \frac{g_{V\rho^0\eta}}{\gamma_V} \cdot \frac{m_V^2}{D_V(q^2)} \cdot \frac{g_{\rho^0\eta\gamma}}{D_\rho(q^2)} \\ F_\omega^{\eta\eta\gamma} &= ie \sum_{V=\omega,\phi,\dots} \frac{g_{V\omega\eta}}{\gamma_V} \cdot \frac{m_V^2}{D_V(q^2)} \cdot \frac{g_{\omega\eta\gamma}}{D_\omega(q^2)} \\ F_\phi^{\eta\eta\gamma} &= ie \sum_{V=\omega,\phi,\dots} \frac{g_{V\phi\eta}}{\gamma_V} \cdot \frac{m_V^2}{D_V(q^2)} \cdot \frac{g_{\phi\eta\gamma}}{D_\phi(q^2)}. \end{aligned} \quad (\text{A1})$$

In the above expressions, the ellipsis in the sum over V s -channel resonances includes all possible radial excitations of vector mesons. For identical pseudoscalar mesons in the final state, one needs to exchange $q_1 \leftrightarrow q_2$ in the decay amplitudes, with the corresponding $q' \leftrightarrow q''$

two-particle momenta. Note that for nonidentical particles ($\pi^0\eta$), the form factors for exchanged mesons are not given by the simple exchange of momenta because of the different isospin of π^0 (isovector) and η (isoscalar) mesons.

-
- [1] G. Bennett *et al.* (Muon $g-2$ Collaboration), *Phys. Rev. D* **73**, 072003 (2006).
- [2] B. Abi *et al.* (Muon $g-2$ Collaboration), *Phys. Rev. Lett.* **126**, 141801 (2021).
- [3] T. Aoyama *et al.*, *Phys. Rep.* **887**, 1 (2020).
- [4] M. Davier, A. Hoecker, B. Malaescu, and Z. Zhang, *Eur. Phys. J. C* **77**, 827 (2017).
- [5] A. Keshavarzi, D. Nomura, and T. Teubner, *Phys. Rev. D* **97**, 114025 (2018).
- [6] G. Colangelo, M. Hoferichter, and P. Stoffer, *J. High Energy Phys.* **02** (2019) 006.
- [7] M. Hoferichter, B. Hoid, and B. Kubis, *J. High Energy Phys.* **08** (2019) 137.
- [8] M. Davier, A. Hoecker, B. Malaescu, and Z. Zhang, *Eur. Phys. J. C* **80**, 241 (2020).
- [9] A. Keshavarzi, D. Nomura, and T. Teubner, *Phys. Rev. D* **101**, 014029 (2020).
- [10] A. Kurz, T. Liu, P. Marquard, and M. Steinhauser, *Phys. Lett. B* **734**, 144 (2014).
- [11] K. Melnikov and A. Vainshtein, *Phys. Rev. D* **70**, 113006 (2004).
- [12] P. Masjuan and P. Sanchez-Puertas, *Phys. Rev. D* **95**, 054026 (2017).
- [13] G. Colangelo, M. Hoferichter, M. Procura, and P. Stoffer, *J. High Energy Phys.* **04** (2017) 161.
- [14] M. Hoferichter, B.-L. Hoid, B. Kubis, S. Leupold, and S. P. Schneider, *J. High Energy Phys.* **10** (2018) 141.
- [15] A. Gérardin, H. B. Meyer, and A. Nyffeler, *Phys. Rev. D* **100**, 034520 (2019).
- [16] J. Bijnens, N. Hermansson-Truedsson, and A. Rodríguez-Sánchez, *Phys. Lett. B* **798**, 134994 (2019).
- [17] G. Colangelo, F. Hagelstein, M. Hoferichter, L. Laub, and P. Stoffer, *J. High Energy Phys.* **03** (2020) 101.
- [18] G. Colangelo, M. Hoferichter, A. Nyffeler, M. Passera, and P. Stoffer, *Phys. Lett. B* **735**, 90 (2014).
- [19] T. Aoyama, M. Hayakawa, T. Kinoshita, and M. Nio, *Phys. Rev. Lett.* **109**, 111808 (2012).
- [20] A. Czarnecki, W. J. Marciano, and A. Vainshtein, *Phys. Rev. D* **67**, 073006 (2003).
- [21] C. Griendiger, D. Stöckinger, and H. Stöckinger-Kim, *Phys. Rev. D* **88**, 053005 (2013).
- [22] R. L. Workman *et al.* (Particle Data Group), *Prog. Theor. Exp. Phys.* **2022**, 083C01 (2022).
- [23] F. Jegerlehner, *EPJ Web Conf.* **166**, 00022 (2018).
- [24] M. Benayoun, L. DelBuono, and F. Jegerlehner, *Eur. Phys. J. C* **82**, 184 (2022).
- [25] M. Abe *et al.*, *Prog. Theor. Exp. Phys.* **2019**, 053C02 (2019).
- [26] M. Aiba *et al.*, [arXiv:2111.05788](https://arxiv.org/abs/2111.05788).
- [27] S. Borsanyi *et al.*, *Nature* (London) **593**, 51 (2021).
- [28] B. Moussallam, *Eur. Phys. J. C* **73**, 2539 (2013).
- [29] M. N. Achasov *et al.*, *Phys. Lett. B* **537**, 201 (2002).
- [30] R. R. Akhmetshin *et al.* (CMD-2 Collaboration), *Phys. Lett. B* **580**, 119 (2004).
- [31] G. Isidori, L. Maiani, M. Nicolaci, and S. Pacetti, *J. High Energy Phys.* **05** (2006) 049.
- [32] A. Aloisio *et al.* (KLOE Collaboration), *Phys. Lett. B* **536**, 209 (2002).
- [33] F. Ambrosino *et al.* (KLOE Collaboration), *Phys. Lett. B* **681**, 5 (2009).
- [34] J. Lu and B. Moussallam, *Eur. Phys. J. C* **80**, 436 (2020).
- [35] B. Moussallam, *Eur. Phys. J. C* **81**, 993 (2021).
- [36] A. Bramon, R. Escribano, J. L. Lucio M., M. Napsuciale, and G. Pancheri, *Phys. Lett. B* **494**, 221 (2000).
- [37] A. Bramon, R. Escribano, J. L. Lucio Martinez, and M. Napsuciale, *Phys. Lett. B* **517**, 345 (2001).
- [38] A. Bramon, R. Escribano, J. L. Lucio M., M. Napsuciale, and G. Pancheri, *Eur. Phys. J. C* **26**, 253 (2002).
- [39] R. J. Eden, P. V. Landshoff, D. I. Olive, and J. C. Polkinghorne, *The Analytic S-Matrix* (Cambridge University Press, Cambridge, England, 1966).
- [40] R. G. Stuart, *Phys. Lett. B* **262**, 113 (1991).
- [41] C. Bouchiat and L. Michel, *J. Phys. Radium* **22**, 121 (1961).
- [42] L. Durand, *Phys. Rev.* **128**, 441 (1962).
- [43] M. Gourdin and E. De Rafael, *Nucl. Phys.* **B10**, 667 (1969).
- [44] G. Calderon and G. Lopez Castro, *Int. J. Mod. Phys. A* **23**, 3525 (2008).
- [45] N. N. Achasov and V. N. Ivanchenko, *Nucl. Phys.* **B315**, 465 (1989).
- [46] N. N. Achasov and A. V. Kiselev, *Phys. Rev. D* **68**, 014006 (2003).
- [47] M. N. Achasov *et al.*, *Phys. Lett. B* **479**, 53 (2000).
- [48] M. N. Achasov *et al.*, *Eur. Phys. J. C* **80**, 1008 (2020).
- [49] M. N. Achasov *et al.* (SND Collaboration), *Eur. Phys. J. C* **82**, 168 (2022).
- [50] M. N. Achasov *et al.*, *Phys. Rev. D* **88**, 054013 (2013).
- [51] M. N. Achasov *et al.*, *Phys. Rev. D* **94**, 112001 (2016).
- [52] M. Hoferichter, B. Kubis, S. Leupold, F. Niecknig, and S. P. Schneider, *Eur. Phys. J. C* **74**, 3180 (2014).
- [53] A. Bramon, R. Escribano, and M. Scadron, *Phys. Lett. B* **503**, 271 (2001).
- [54] R. Escribano and E. Royo, *Phys. Lett. B* **807**, 135534 (2020).
- [55] V. M. Aulchenko *et al.*, *J. Exp. Theor. Phys.* **121**, 27 (2015).
- [56] S. S. Gribov *et al.*, *J. High Energy Phys.* **01** (2020) 112.
- [57] M. N. Achasov *et al.*, *Phys. Rev. D* **99**, 112004 (2019).

- [58] B. Aubert *et al.* (BABAR Collaboration), *Phys. Rev. D* **77**, 092002 (2008).
- [59] M. Ablikim *et al.* (BESIII Collaboration), *Phys. Lett. B* **813**, 136059 (2021).
- [60] F. Ambrosino *et al.*, *Eur. Phys. J. C* **49**, 473 (2006).
- [61] I. Caprini, G. Colangelo, and H. Leutwyler, *Phys. Rev. Lett.* **96**, 132001 (2006).
- [62] R. García-Martín, R. Kamiński, J. R. Peláez, and J. R. de Elvira, *Phys. Rev. Lett.* **107**, 072001 (2011).
- [63] D. Bisello *et al.* (DM2 Collaboration), *Nucl. Phys. B, Proc. Suppl.* **21**, 111 (1991).
- [64] F. E. Close and N. A. Tornqvist, *J. Phys. G* **28**, R249 (2002).
- [65] C. Amsler and N. A. Tornqvist, *Phys. Rep.* **389**, 61 (2004).
- [66] D. Bugg, *Phys. Rep.* **397**, 257 (2004).
- [67] E. Klempt and A. Zaitsev, *Phys. Rep.* **454**, 1 (2007).
- [68] B. M. K. Nefkens *et al.* (A2 at MAMI), *Phys. Rev. C* **90**, 025206 (2014).
- [69] S. Prakhov *et al.*, *Phys. Rev. C* **78**, 015206 (2008).
- [70] S. J. Brodsky and E. de Rafael, *Phys. Rev.* **168**, 1620 (1968).
- [71] B. E. Lautrup and E. de Rafael, *Phys. Rev.* **174**, 1835 (1968).